Surface properties of neutron-rich exotic nuclei within relativistic mean field formalisms

M. Bhuyan,[1,2,*] B. V. Carlson,[1,†] S. K. Patra,[3] and Shan-Gui Zhou[2,4,5]

[1]*Instituto Tecnológico de Aeronáutica, 12.228-900 São José dos Campos, São Paulo, Brazil*
[2]*Key Laboratory of Theoretical Physics, Institute of Theoretical Physics, Chinese Academy of Sciences, Beijing 100190, China*
[3]*Institute of Physics, Sachivalaya Marg, Sainik School, Bhubaneswar 751005, India*
[4]*Center of Theoretical Nuclear Physics, National Laboratory of Heavy Ion Accelerator, Lanzhou 730000, China*
[5]*Synergetic Innovation Center for Quantum Effects and Application, Hunan Normal University, Changsha 410081, China*

In this theoretical study, we establish a correlation between the neutron skin thickness and the nuclear symmetry energy for the even-even isotopes of Fe, Ni, Zn, Ge, Se, and Kr within the framework of the axially deformed self-consistent relativistic mean field for the nonlinear NL3* and density-dependent DD-ME1 interactions. The coherent density functional method is used to formulate the symmetry energy, the neutron pressure, and the curvature of finite nuclei as a function of the nuclear radius. We have performed broad studies for the mass dependence on the symmetry energy in terms of the neutron-proton asymmetry for mass $70 \leqslant A \leqslant 96$. From this analysis, we found a notable signature of a shell closure at $N = 50$ in the isotopic chains of Fe, Ni, Zn, Ge, Se, and Kr nuclei. The present study reveals a interrelationship between the characteristics of infinite nuclear matter and the neutron skin thickness of finite nuclei.

I. INTRODUCTION

Investigation of nuclei far from the line of β-stability has played a significant role in nuclear physics. Further, the advancement in the experimental facilities such as Jyaväskylä (Finland) [1], ORNL (United States) [2], CSR (China) [3], FAIR (Germany) [4], RIKEN (Japan) [5], GANIL (France) [6], GSI (Germany) [7], FLNR (Russia) [8], and FRIB (United States) [9] has already opened new possibilities of exploring the production of various exotic nuclei and their properties under the extreme conditions of large isospin asymmetry. By virtue of the neutron-proton asymmetry in finite nuclei, one can gain insight into some of the basic components of the equation of state (EoS) of nuclear matter such as the symmetry energy S_0 (ρ) and the slope parameter L_0 (ρ) at nuclear saturation density ρ_0 [10]. In other words, the density properties of the symmetry energy of nuclear matter is forced to lie within a narrow window in terms of the nuclear bulk properties of neutron rich nuclei and vice-versa [11]. In this context, a better understanding of the isospin and density dependent of the symmetry energy in exotic nuclei is one of the primary objectives of present studies.

Exploring the nuclear surface properties of semi-infinite nuclear matter is simple as compared to a finite nuclear system due to the absence of the many complexities arising from the shell, the charge, occupation probability, and finite-size effects. In past works, the semiclassical Thomas-Fermi model [12–14], and quantal Hartree-Fock approach [15,16] have investigated the surface properties of symmetric as well as asymmetric nuclear matter. Recently, considering the isotopic chains of doubly close shell nuclei, Warda *et al.* have demonstrated theoretically that the stiffness of the symmetry energy is dependent on the bulk and the surface component of the neutron skin thickness [17–19]. Furthermore, the correlation between the volume and surface symmetry energy for finite nuclei has been extensively discussed in Refs. [20–25]. In addition to these, the effects of temperature on the surface and the bulk symmetry have also been reported recently [26,27]. In these works, the surface symmetry energy term is predicted to be more sensitive to the temperature than that of the volume one [26,27]. The symmetry energy is not a directly measurable quantity but its value can be estimated indirectly from physical observables that are correlated to it. Two constraints are the experimental energy of the giant dipole resonance [28] and the experimental differential cross-section data in a charge exchange reaction using the isospin dependent interaction of the optical potential [29,30] (see the recent review of the Refs. [31,32] for details). Further, the connection of isospin asymmetry to the symmetry energy has an impact on many physical studies such as astrophysical observations [33–38], the ground state structure of exotic nuclei [39–42], the determination of the neutron skin [43,44], the dynamics of heavy-ion reactions [45–47], giant collective excitations [48,49], the dipole polarizability [50–53], the mirror charge radii [54,55], the properties of compact star object [20,37,38,56], the nucleosynthesis process through neutrino convection [25,57], the photospheric radius of a neutron star [25], the core collapse of compact massive stars and related explosive phenomena at high density [20,58].

At present, a concerted effort has been put forth to determine the density properties of the symmetry energy and slope parameters for highly neutron-proton asymmetric systems in nuclear matter and in drip-line nuclei [59–63]. Broadly, these nuclear matter parameters are involved in the bulk properties of finite

nuclei such as binding energies [27,59,64], relative nuclear radii [64–67], and neutron density distributions [59,60,64,67]. In this theoretical investigation, we study the relation between the neutron skin thickness and nuclear matter properties at saturation density, such as the symmetry energy, the neutron pressure, and the curvature in an isotopic chain. Furthermore, we demonstrate in a few cases a relation between various bulk physical quantities of finite nuclei and the density properties of infinite nuclear matter. We consider the neutron rich even-even isotopes of medium mass nuclei such as Fe, Ni, Zn, Ge, Se, and Kr in the present analysis, as they are primary candidates in the the upcoming experimental facilities and several predictions have been made for them regarding the emergence of a nuclear skin. The calculations are performed within the axially deformed relativistic mean field approach, which has the ability to predict the nuclear skin thickness in exotic nuclei [66,68,69]. To interlink the infinite nuclear matter properties to intrinsic finite nuclear bulk properties, we have used the coherent density functional method [63,64,70–72] through the energy density functional of Brueckner *et al.* [73,74]. Briefly, our aim to constrain the nuclear matter observables using the inherent properties of exotic neutron rich finite nuclei as well as the contrary.

This paper is organized as follows. In Sec. II we discuss the theoretical model for the relativistic mean field approach along with coherent density functional method. Section III is assigned to the discussion of the results obtained from our calculation and of the possible correlation among the infinite nuclear matter and finite nucleus properties. Finally, a summary and a brief conclusion are given in Sec. IV.

II. THEORETICAL FORMALISM

In the present work, we estimate the nuclear symmetry energy $S_0(\rho)$, neutron pressure $p_0(\rho)$, and other related physical quantities of exotic finite nuclei as functions of the baryon density on the basis of the corresponding definitions for asymmetric nuclear matter. We have taken a general form of the nonlinear finite-range relativistic mean field model, considering it to be represented by the Lagrangian density (given in the next subsection) [66,75,76]. This model has been widely used to describe infinite nuclear matter, finite nuclei, and stellar matter properties for extreme isospin asymmetry [39,66,75–93]. To calculate the effective intrinsic nuclear matter quantities in finite nuclei, one must know the key parameters of nuclear matter that characterize its density dependence at saturation density. The most general form of the nuclear matter symmetry energy $S(\rho)$ for the relativistic mean field models can be expressed as

$$S^{NM}(\rho) = \frac{1}{8}\left(\frac{\partial^2(\mathcal{E}/\rho)}{\partial y^2}\right)_{\rho,y=1/2}, \qquad (1)$$

where y is the proton fraction for asymmetric nuclear matter. Here, the detailed calculations of the energy density $\mathcal{E}$ as a function of density from the relativistic Lagrangian are given in Refs. [37,90,91,94,95]. The widely used slope parameter

TABLE I. Parameters and infinite nuclear matter properties at saturation density of the nonlinear NL3* [97] and density-dependent DD-ME1 [90] interaction parameters.

NL3* interaction [97]	DD-ME1 interaction [90]
$M = 939$	$M = 939$
$m_\sigma = 502.5742$	$m_\sigma = 549.5255$
$m_\omega = 782.6000$	$m_\omega = 783.0000$
$m_\rho = 763.000$	$m_\rho = 763.000$
$m_\sigma = 10.0944$	$m_\sigma\ (\rho_{\rm sat}) = 10.4434$
$m_\omega = 12.8065$	$m_\omega\ (\rho_{\rm sat}) = 12.8939$
$m_\rho = 4.5748$	$m_\rho\ (\rho_{\rm sat}) = 3.8053$
$g_2 = -10.8093$	$a_\sigma = 1.3854$
$g_3 = -30.1486$	$b_\sigma = 0.9781$
$M/M^* = 0.594$	$c_\sigma = 1.5342$
$\rho_0 = 0.150$	$d_\sigma = 0.4661$
$\mathcal{E}/\mathcal{A} = -16.31$	$a_\omega = 1.3879$
$K_0^{NM} = 258.27$	$b_\omega = 0.8525$
$S^{NM} = 38.68$	$c_\omega = 1.3566$
	$d_\omega = 0.4957$
	$a_\rho = 0.5008$
	$M/M^* = 0.586$
	$\rho_0 = 0.152$
	$\mathcal{E}/\mathcal{A} = -16.04$
	$K_0^{NM} = 244.72$
	$S^{NM} = 33.06$

L^{NM} at saturation density is given as

$$L_0^{NM} = 3\rho\left(\frac{\partial S^{NM}}{\partial \rho}\right)_{\rho=\rho_0} = \frac{3p_0^{NM}}{\rho_0}, \qquad (2)$$

where p_0^{NM} is the neutron pressure of nuclear matter at saturation density, ρ_0 being the saturation density of the symmetric nuclear matter. Further, the curvature and skewness of the symmetry energy are given by

$$K_0^{NM} = 9\rho^2\left(\frac{\partial^2 S^{NM}}{\partial \rho^2}\right)_{\rho=\rho_0} \qquad (3)$$

and

$$Q_0^{NM} = 27\rho^3\left(\frac{\partial^3 S^{NM}}{\partial \rho^3}\right)_{\rho=\rho_0}, \qquad (4)$$

respectively. Our present knowledge of the basic properties of the symmetry energy around saturation density is still poor with its value estimated to be about 27 ± 3 MeV [94,96]. In practice, this ambiguity play an essential role in the structure calculations of finite nuclei. Here, to obtain a general idea of what one might expect, we have used the calculated saturation properties of infinite nuclear matter from the relativistic mean field with nonlinear NL3* and density-dependent DD-ME1 interaction parameters, which are listed in Table I (for details see Refs. [37,90,91,97]). In the relativistic mean field (RMF) model, there is a strong correlation between the Dirac effective nucleon mass at saturation density and the strength of the spin-orbit force in finite nuclei [98,99]. Further, one of the most compelling features of RMF models is the reproduction of the spin-orbit splittings in finite nuclei. This occurs when the velocity dependence of the equivalent central potential that leads to saturation arises primarily due to a reduced nucleon effective

mass [100]. On the other hand, the nonrelativistic effective mass parametrizes the momentum dependence of the single-particle potential, which is the result of a quadratic parametrization of the single-particle spectrum. It has been argued [101] that the so-called Lorentz mass should be compared with the nonrelativistic effective mass extracted from analyses carried out in the framework of nonrelativistic optical and shell models.

A. The relativistic mean-field theory

The fundamental theory of the strong interaction that can provide a complete description of nuclear equation of state is quantum chromodynamics (QCD). At present, it is not conceivable to describe the complete picture of hadronic matter due to its nonperturbative properties. Hence, one needs to apply the perspective of an effective field theory (EFT) at low energy, such as quantum hadrodynamics (QHD) [75–77]. The mean field treatment of QHD has been used widely to describe the properties of infinite nuclear matter [37,38,76,91] and finite nuclei [42,75,77,79,80,90,93]. In the relativistic mean field approach, the nucleus is considered as a composite system of nucleons (proton and neutron) interacting through the exchange of mesons and photons [76,81–85,102]. Further, the contributions from the meson fields are described either by mean fields or by point-like interactions between the nucleons [103,104]. Density dependent coupling constants [39,89–93] and/or nonlinear coupling terms [75,105] are introduced to reproduced the properties of finite nuclei and the correct saturation properties of infinite nuclear matter. Here, most of the computational effort is devoted to solving the Dirac equation and calculating various densities. In the present calculation, we have used the microscopic self-consistent relativistic mean field (RMF) theory as a standard tool to investigate nuclear structure. It is worth mentioning that the RMF approach is one of the most popular and widely used formalisms. A typical relativistic Lagrangian density (after several modifications of the original Walecka Lagrangian to take care of various limitations) for a nucleon-meson many body system has the form [75,76,78–88]

$$
\begin{aligned}
\mathcal{L} = &\ \overline{\psi}\{i\gamma^\mu \partial_\mu - M\}\psi + \frac{1}{2}\partial^\mu \sigma \partial_\mu \sigma \\
&- \frac{1}{2}m_\sigma^2 \sigma^2 - \frac{1}{3}g_2 \sigma^3 - \frac{1}{4}g_3 \sigma^4 - g_s \overline{\psi}\psi\sigma \\
&- \frac{1}{4}\Omega^{\mu\nu}\Omega_{\mu\nu} + \frac{1}{2}m_w^2 \omega^\mu \omega_\mu - g_w \overline{\psi}\gamma^\mu \psi \omega_\mu \\
&- \frac{1}{4}\vec{B}^{\mu\nu}.\vec{B}_{\mu\nu} + \frac{1}{2}m_\rho^2 \vec{\rho}^\mu.\vec{\rho}_\mu - g_\rho \overline{\psi}\gamma^\mu \vec{\tau}\psi \cdot \vec{\rho}^\mu \\
&- \frac{1}{4}F^{\mu\nu}F_{\mu\nu} - e\overline{\psi}\gamma^\mu \frac{(1-\tau_3)}{2}\psi A_\mu
\end{aligned}
\tag{5}
$$

with vector field tensors

$$
\begin{aligned}
F^{\mu\nu} &= \partial_\mu A_\nu - \partial_\nu A_\mu, \\
\Omega_{\mu\nu} &= \partial_\mu \omega_\nu - \partial_\nu \omega_\mu, \\
\vec{B}^{\mu\nu} &= \partial_\mu \vec{\rho}_\nu - \partial_\nu \vec{\rho}_\mu.
\end{aligned}
\tag{6}
$$

Here, the field for the σ meson is denoted by σ, that for the ω meson by ω_μ, and for the isovector ρ meson by $\vec{\rho}_\mu$. The

electromagnetic field is defined by A_μ. The quantities, $\Omega^{\mu\nu}$, $\vec{B}_{\mu\nu}$, and $F^{\mu\nu}$ are the field tensors for the ω^μ, $\vec{\rho}_\mu$, and photon fields, respectively.

The RMF model proposed in Refs. [90,91] allows density dependence of the meson-nucleon coupling, which is parametrized in a phenomenological approach [39,89–93]. The coupling of the mesons to the nucleon fields are defined as

$$
g_i(\rho) = g_i(\rho_{\text{sat}})f_i(x)|_{i=\sigma,\omega},
\tag{7}
$$

where

$$
f_i(x) = a_i \frac{1 + b_i(x + d_i)^2}{1 + c_i(x + d_i)^2}
\tag{8}
$$

and

$$
g_\rho = g_\rho(\rho_{\text{sat}})e^{a_\rho(x-1)}.
\tag{9}
$$

Here, the functional $x = \rho/\rho_{\text{sat}}$ and the eight real parameters in Eq. (8) are not independent. The five constraints $f_i(1) = 1$, $f_\sigma''(1) = f_\omega''(1)$, and $f_i''(0) = 0$ reduce the number of independent parameters to three. These independent parameters (coupling parameters and the mass of the σ meson) were adjusted to reproduce the properties of symmetric and asymmetric nuclear matter and the ground state properties of finite nuclei.

From the above Lagrangian density we obtain the field equations for the nucleons and the mesons. These equations are solved by expanding the upper and lower components of the Dirac spinors and the boson fields in an axially deformed harmonic oscillator basis, with an initial deformation β_0. The set of coupled equations is solved numerically by a self-consistent iteration method. The center-of-mass motion energy correction is estimated by the usual harmonic oscillator formula $E_{\text{c.m.}} = \frac{3}{4}(41A^{-1/3})$. The quadrupole deformation parameter β_2 is evaluated from the resulting proton and neutron quadrupole moments, as

$$
Q = Q_n + Q_p = \sqrt{\frac{16\pi}{5}}\left(\frac{3}{4\pi}AR^2\beta_2\right).
\tag{10}
$$

The root mean square (rms) matter radius is defined as

$$
\langle r_m^2 \rangle = \frac{1}{A}\int \rho(r_\perp,z)r^2 d\tau,
\tag{11}
$$

where A is the mass number, and $\rho(r_\perp,z)$ is the deformed density. The total binding energy and other observables are also obtained by using the standard relations, given in Ref. [99]. Here, we have used the NL3* [97,106] and the density-dependent DD-ME1 [90] interactions. These interactions are able to reproduce reasonably well the properties of not only the stable nuclei but also those not too far from the β-stability valley [90,93,97,106]. In the outputs, we obtain the potentials, densities, single-particle energy levels, nuclear radii, deformations, and the binding energies. For a given nucleus, the maximum binding energy corresponds to the ground state and other solutions are obtained as various excited intrinsic states at other deformations, provided the nucleus does not undergo fission.

To describe the nuclear bulk properties of open-shell nuclei, one has to consider the pairing correlations in their ground as well as excited states [107]. There are various methods, such as the BCS approach, the Bogoliubov transformation and particle

number conserving methods, that have been developed to treat pairing effects in the study of nuclear properties including fission barriers [108–111]. In principle, the Bogoliubov transformation is the most widely used method to take pairing correlations into account for the drip-line region [82–85,112,113]. In the case of nuclei not too far from the β-stability line, one can use the constant gap BCS pairing approach to obtain a reasonably good approximation of pairing [114]. In the present analysis, we have employed the constant gap BCS approach with the NL3* and a Bogoliubov transformation with DD-ME1 interactions [42,66,79,90,93,115,116].

B. The coherent density functional method

The coherent density functional method (CDFM) was suggested and developed by Antonov *et al.* [70,71]. It is based on the δ-function limit of the generator coordinate method [63,67,72]. In CDFM, the one-body density matrix ρ ($\mathbf{r}$,$\mathbf{r}'$) of a finite nucleus can be written as a coherent superposition of the one-body density matrices ρ_x ($\mathbf{r}$,$\mathbf{r}'$) for spherical pieces of the nuclear matter called *fluctons*,

$$\rho_x(\mathbf{r}) = \rho_0(x)\Theta(x - |\mathbf{r}|) \tag{12}$$

with $\rho_o(x) = \frac{3A}{4\pi x^3}$. The generator coordinate x is the spherical radius of all A nucleons contained in a uniform distributed spherical Fermi gas. In finite nuclear system, the one body density matrix is given as [63,64,67,72]

$$\rho(\mathbf{r},\mathbf{r}') = \int_0^\infty dx|f(x)|^2\rho_x(\mathbf{r},\mathbf{r}'), \tag{13}$$

where $|f(x)|^2$ is the weight function [defined in Eq. (17)]. The term $\rho_x(\mathbf{r},\mathbf{r}')$ is the coherent superposition of the one-body density matrix and defined as

$$\rho_x(\mathbf{r},\mathbf{r}') = 3\rho_0(x)\frac{J_1(k_f(x)|\mathbf{r} - \mathbf{r}'|)}{(k_f(x)|\mathbf{r} - \mathbf{r}'|)}$$
$$\times \Theta\left(x - \frac{|\mathbf{r} + \mathbf{r}'|}{2}\right). \tag{14}$$

Here, J_1 is the first order spherical Bessel function and $k_F(x)$ is the Fermi momentum of the nucleons in the flucton with radius x. The corresponding Wigner distribution function for the one-body density matrices in Eq. (14) is

$$W(\mathbf{r},\mathbf{k}) = \int_0^\infty dx|f(x)|^2W_x(\mathbf{r},\mathbf{k}), \tag{15}$$

where $W_x(\mathbf{r},\mathbf{k}) = \frac{4}{8\pi^3}\Theta(x - |\mathbf{r}|)\Theta(k_F(x) - |\mathbf{k}|)$. Similarly, the density ρ ($\mathbf{r}$) in the CDFM can express in terms of the same weight function as

$$\rho(r) = \int d\mathbf{k}W(\mathbf{r},\mathbf{k}) = \int_0^\infty dx|f(x)|^2\frac{3A}{4\pi x^3}\Theta(x - |\mathbf{r}|) \tag{16}$$

and it is normalized to the mass number, $\int\rho(\mathbf{r})d\mathbf{r} = A$. By taking the δ-function approximation to the Hill-Wheeler integral equation, one obtains a differential equation for the weight function in the generator coordinate [70–72]. We have adopted a conventional approach to the weight function instead of solving the differential equation (detail in Refs. [71,72]).

The weight function for a given density distribution ρ (r) can be expressed as

$$|f(x)|^2 = -\left(\frac{1}{\rho_0(x)}\frac{d\rho(r)}{dr}\right)_{r=x} \tag{17}$$

with $\int_0^\infty dx|f(x)|^2 = 1$. For a detailed analytical derivation, one can follow Refs. [72,89,105]. Here, our principal goal is to define an effective symmetry energy, its slope, and curvature for a finite nucleus around by weighting the quantities for infinite nuclear matter within the CDFM. Following the CDFM approach, the effective symmetry energy S_0, its corresponding pressure p_0, and the curvature K_0 for a finite nucleus can be written as [63,64,67,72,89,105]

$$S_0 = \int_0^\infty dx|f(x)|^2S^{NM}(\rho(x)),$$
$$p_0 = \int_0^\infty dx|f(x)|^2p_0^{NM}(\rho(x)), \tag{18}$$
$$K_0 = \int_0^\infty dx|f(x)|^2K_0^{NM}(\rho(x)).$$

We will see that the quantities on the left-hand side of Eq. (18) (i.e., symmetry energy S_0, neutron pressure p_0 and the curvature K_0) are surface weighted average of the corresponding nuclear matter quantities S^{NM}, p_0^{NM}, and K_0^{NM} with local density density ρ (x) on the right-hand side. The region within $x_{\min} \leqslant x \leqslant x_{\max}$ (see Fig. 3 displaying the weight function) is taken for the integration. More details can found in Sec. III. The calculated densities from the NL3* and the DD-ME1 are used for estimate the weight function $|f(x)|^2$ in Eq. (17) for each nucleus and used for the calculations in Eq. (18). The spin-independent proton and neutron mean-field densities are given by

$$\rho(\mathbf{R}) = \rho(r_\perp,z), \tag{19}$$

where $r_\perp$ and z are the cylindrical coordinates of the radial vector $\mathbf{R}$. The single particle densities are

$$\rho_i(\mathbf{R}) = \rho_i(r_\perp,z) = |\phi_i^+(r_\perp,z)|^2 + |\phi_i^-(r_\perp,z)|^2, \tag{20}$$

where $\phi_i^\pm$ is the wave function, expanded into the eigenfunctions of an axially symmetric deformed harmonic oscillator potential in cylindrical co-ordinates. The normalization of the densities is given by

$$\int \rho(\mathbf{R})d\mathbf{R} = X, \tag{21}$$

where $X = N, Z$ for neutron and proton number, respectively. Further, the multipole decomposition of the density can be written in terms of even values of the multipole index λ as

$$\rho(r_\perp,z) = \sum_\lambda \rho_i(\mathbf{R})P_\lambda(\cos\theta). \tag{22}$$

Here, we have used the monopole term of the density distribution in the expansion Eq. (22) for the calculation of the weight function $|f(x)|^2$ for simplicity. For a deformed nucleus, the peak of $|f(x)|^2$ does indeed depend on the angle. However, the density also depends on the angle in such a manner that the density at the peak of $|f(x)|^2$ is almost constant. The

TABLE II. The binding energy (BE), charge radius r_{ch}, and the quadrupole deformation parameter β_2 for the ground states of the $^{72-86}$Fe, $^{74-88}$Ni, and $^{76-90}$Zn nuclei from the nonlinear NL3* and the density dependent DD-ME1 calculations compare with the experimental data [117–119], wherever available. The asterisk (*) marks in the binding energies of the experimental data are for extrapolated values.

Nucleus	Binding energy			Charge radius			Quadrupole deformation		
	NL3*	DD-ME1	Expt. [117]	NL3*	DD-ME1	Expt. [118]	NL3*	DD-ME1	Expt. [119]
^{70}Fe	580.68	580.59	577.43*	3.875	3.879	––	0.179	0.190	––
^{72}Fe	588.89	588.68	589.10*	3.898	3.899	––	0.207	0.214	––
^{74}Fe	594.98	594.78	––	3.912	3.909	––	0.198	0.188	––
^{76}Fe	600.61	600.58	––	3.938	3.935	––	0.004	0.002	––
^{78}Fe	602.99	603.65	––	3.956	3.950	––	0.261	0.254	––
^{80}Fe	605.64	606.70	––	3.958	3.966	––	0.211	0.248	––
^{82}Fe	608.40	609.21	––	3.978	3.979	––	0.223	0.225	––
^{84}Fe	609.37	611.02	––	3.994	3.992	––	0.202	0.188	––
^{86}Fe	610.40	612.64	––	4.006	3.995	––	0.174	0.124	––
^{72}Ni	611.78	612.34	613.15	3.901	3.892	––	0.042	0.014	––
^{74}Ni	621.94	622.31	623.74*	3.923	3.908	––	0.099	0.096	0.21*
^{76}Ni	630.95	631.52	633.16*	3.929	3.923	––	0.009	0.006	––
^{78}Ni	635.85	635.96	641.94*	3.945	3.935	––	0.001	0.002	––
^{80}Ni	643.51	643.61	––	3.958	3.954	––	0.008	0.011	––
^{82}Ni	646.72	645.74	––	3.974	3.967	––	0.091	0.096	––
^{84}Ni	649.67	650.64	––	3.990	3.982	––	0.085	0.059	––
^{86}Ni	652.52	653.84	––	3.995	3.994	––	0.067	0.035	––
^{88}Ni	655.08	656.76	––	4.007	4.010	––	0.034	0.005	––
^{74}Zn	637.64	637.27	639.51	3.985	3.981	––	0.161	0.185	––
^{76}Zn	650.78	650.51	652.08	4.001	3.997	––	0.182	0.201	––
^{78}Zn	661.39	661.01	663.44	4.008	4.006	––	0.150	0.164	––
^{80}Zn	670.90	670.99	674.08	4.009	4.010	––	0.001	0.002	––
^{82}Zn	677.13	677.08	680.84*	4.039	4.042	––	0.151	0.186	––
^{84}Zn	682.51	682.59	––	4.069	4.069	––	0.202	0.216	––
^{86}Zn	687.54	687.68	––	4.096	4.095	––	0.230	0.238	––
^{88}Zn	691.09	691.76	––	4.119	4.117	––	0.228	0.227	––
^{90}Zn	694.32	695.42	––	4.136	4.136	––	0.213	0.206	––

effect of the multipole component in the expansion can thus be neglected. We can define the neutron skin thickness ΔR using the root-mean-square (rms) radii of neutrons and protons as

$$\Delta R = \langle r_n^2 \rangle - \langle r_p^2 \rangle. \qquad (23)$$

The quantities defined above in Eq. (23) are used in the present study.

III. CALCULATIONS AND RESULTS

In the relativistic mean field model, the field equations are solved self-consistently by taking different inputs for the initial deformation β_0 [77,79,90,93,97,99,106]. To verify the convergence of the ground state solutions for this mass region, we performed calculations for the number of major boson shells $N_B = 16$ and varied the number of major fermion shells N_F from 10 to 20. From the results obtained, we have confirmed that the relative variations of these solutions are $\leqslant 0.004\%$ for the binding energy and 0.001% for the nuclear radii over the range of major fermion shells. Hence, the desired number of major shells for fermions and bosons were fixed at $N_F = 16$ and $N_B = 16$. The number of mesh points for Gauss-Hermite and Gauss-Laguerre integration used are 20 and 24, respectively. For a given nucleus, the solution

corresponding to the maximum binding energy is treated as the ground state and other solutions are considered excited states of the nucleus. We have used the nonlinear NL3* [97] and density-dependent DD-ME1 [90] interactions for the present analysis. These interaction parameters are widely used and are able to provide a reasonable good description of the properties of nuclei from light to superheavy, from the proton to the neutron drip line [42,79,80,97]. The calculations furnish the ground state bulk properties such as binding energy, rms charge radius, nuclear quadrupole deformation β_2, nuclear density distribution $\rho(r_\perp, z)$, and the single particle energy.

The results obtained from both sets of interaction parameters along with the experimental data [117–119] are listed in Tables II and III. From the tables, one notices that the results of our calculations agree quite well with the experimental data for binding energy and root-mean-square charge radius, wherever available. In both the NL3* and DD-ME1 results, we find deformed prolate solutions in the ground state configuration for entire isotopic chains except the mass region near $N = 50$. In other words, the deformed prolate configuration follows a spherical solution at $N = 50$ and again becomes deformed with increasing neutron number for the Fe, Zn, Ge, Se, and Kr nuclei. In the case of the isotopic chain of Ni, we found almost spherical solutions for the entire isotopic chain, which

TABLE III. The binding energy (BE), charge radius r_{ch}, and the quadrupole deformation parameter β_2 for the ground states of the $^{78-92}$Ge, $^{80-94}$Se, and $^{82-96}$Kr nuclei for the nonlinear NL3* and the density dependent DD-ME1 calculations compare with the experimental data [117–119], wherever available. The asterisk (*) marks in the binding energies of the experimental data are for extrapolated values.

Nucleus	Binding energy			Charge radius			Quadrupole deformation		
	NL3*	DD-ME1	Expt. [117]	NL3*	DD-ME1	Expt. [118]	NL3*	DD-ME1	Expt. [119]
^{76}Ge	658.59	657.85	661.59	4.052	4.050	4.0811	0.171	0.179	——
^{78}Ge	674.41	673.71	676.38	4.064	4.061	——	0.181	0.189	0.2623
^{80}Ge	688.05	687.64	690.18	4.071	4.066	——	0.158	0.164	——
^{82}Ge	699.53	699.56	702.43	4.068	4.068	——	0.001	0.012	——
^{84}Ge	707.17	706.87	711.22*	4.099	4.101	——	0.153	0.181	——
^{86}Ge	714.42	714.24	——	4.131	4.132	——	0.207	0.216	——
^{88}Ge	721.25	721.22	——	4.160	4.161	——	0.235	0.244	——
^{90}Ge	726.52	726.92	——	4.184	4.185	——	0.235	0.236	——
^{92}Ge	731.42	732.04	——	4.206	4.208	——	0.225	0.224	——
^{78}Se	676.63	675.80	679.98	4.113	4.110	4.1406	0.162	0.181	0.2712
^{80}Se	694.77	693.95	696.86	4.122	4.119	4.1400	0.173	0.185	0.2318
^{82}Se	710.82	710.33	712.84	4.128	4.126	4.1400	0.154	0.170	0.1934
^{84}Se	725.73	725.51	727.34	4.123	4.117	——	0.001	0.001	——
^{86}Se	733.52	733.21	738.07	4.141	4.151	——	0.032	0.045	——
^{88}Se	743.26	742.34	747.55	4.185	4.187	——	0.202	0.215	——
^{90}Se	751.63	751.42	755.73*	4.216	4.214	——	0.237	0.247	——
^{92}Se	758.96	759.01	762.58*	4.241	4.240	——	0.239	0.243	——
^{94}Se	765.53	765.85	768.92*	4.266	4.266	——	0.232	0.236	——
^{80}Kr	691.74	691.08	695.43	4.164	4.158	4.1970	0.095	0.097	0.2650
^{82}Kr	711.77	710.96	714.27	4.171	4.167	4.1919	0.124	0.126	0.2021
^{84}Kr	730.13	729.56	732.25	4.171	4.171	4.1884	0.078	0.097	0.1489
^{86}Kr	747.73	747.56	749.23	4.174	4.170	4.1835	0.001	0.001	——
^{88}Kr	757.48	756.93	761.80	4.192	4.195	4.2171	0.027	0.105	——
^{90}Kr	767.61	767.18	773.22	4.227	4.228	4.2423	0.158	0.173	——
^{92}Kr	777.57	777.49	783.18	4.261	4.269	4.2724	0.210	0.236	——
^{94}Kr	786.29	786.47	791.67*	4.286	4.289	4.3002	0.218	0.222	——
^{96}Kr	794.34	794.75	799.68*	4.307	4.311	4.3267	0.206	0.208	——

do not appear in case of other nuclei (see Tables II and III). The experimental data for the deformations are slightly underestimated by the calculations for both sets of interaction parameters.

A. The neutron separation energy

The two neutron separation energy S_{2n} (Z,N) can be estimated from the ground state nuclear masses BE (Z,N) and BE $(Z, N-2)$ and the neutron mass m_n by the relation

$$S_{2n}(Z,N) = -BE(Z,N) + BE(Z,N-2) + 2m_n. \quad (24)$$

The BE of the $^A Z$ and $^{A-2} Z$ nuclei are calculated using the nonlinear NL3* and the density-dependent DD-ME1 interaction parameters. Here, we have used the experimental data [117] to obtain the experimental values of the S_{2n} energy for comparison with our calculated results. From Tables II and III, one observes that the calculated binding energies are reasonably good agreement with the available experimental data, which shows the predictive power of the calculations for the correct evolution of shell structures. The estimated S_{2n} results along with the experimental values (wherever available) are shown in the upper panel of Fig. 1 for $^{70-86}$Fe, $^{72-88}$Ni, $^{74-90}$Zn, $^{76-92}$Ge, $^{78-94}$Se, and $^{80-96}$Kr isotopes. The

two-neutron separation energy S_{2n}, as a function of the neutron number in an isotopic chain, decreases smoothly as the number
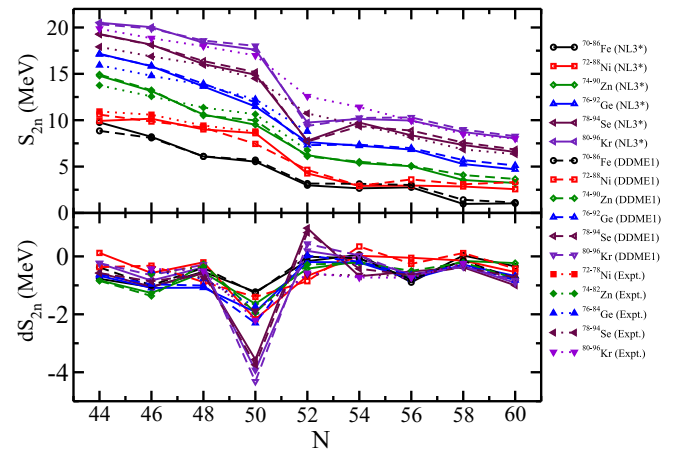

FIG. 1. The two neutron separation energies S_{2n} (upper panel) and the differential variation of the separation energy dS_{2n} (lower panel) from the NL3* and the DD-ME1 interactions are given for Fe, Ni, Zn, Ge, Se, and Kr isotopic chains. The experimental data [117] are given for comparison, wherever available. See text for details.

of neutron increases. Sharp discontinuities (kinks) appear at the neutron spherical closure magic number $N = 50$. In terms of energy, the energy necessary to remove two neutrons from a nucleus $(Z, N_{magic} + 2)$ is much smaller than that to remove two neutrons from the nucleus (Z, N_{magic}), which breaks the regular trend. From Fig. 1 (upper panel), one can observe that the calculated results are in agree with the experimental data and also follow the expected trend along the isotopic chains.

To better explore the dependence of S_{2n} with respect to neutron number, the differential variation of the S_{2n} $[dS_{2n}(N, Z)]$ is defined as

$$dS_{2n}(Z, N) = \frac{S_{2n}(Z, N + 2) - S_{2n}(Z, N)}{2}. \quad (25)$$

In Fig. 1 (upper panel), we observe that the curves for isotopic chains for different atomic number shows roughly the similar trends. From these general characteristics of the S_{2n} curves we expect that the derivative, dS_{2n}, should have a sharp fall in the negative direction for magic or/and semimagic neutron number in an isotopic chain. In other words, the magnitude of the sharp drop, at magic neutron numbers shows the strength of the shell structure for that specific neutron number in the isotopic chain. Here, we found similar characteristics for the Fe, Ni, Zn, Ge, Se, and Kr nuclei (see the lower panel of Fig. 1). The experimental values [117] are also given for comparison. Further, the depth of dS_{2n} at magic neutron number increases along the isotonic chain. The fall in dS_{2n} at $N = 50$ for the isotopic chain discloses additional nuclear structure features.

B. The nuclear density and weight function

Once we have the density in hand, we estimate the nuclear matter observables using these densities in the framework of the coherent density functional method (CDFM) [63,64,67,70,71], which involves the following steps: (i) we generate the weight function $|f(x)|^2$ for each nucleus using the density distribution obtained from the RMF (NL3* and DD-ME1), as defined in Eq. (17) [63,64,67,70,71], (ii) then we use this weight function along with the nuclear matter observables to calculate the effective symmetry energy properties in finite nuclei [63,64,67,70,71]. We compare our calculated results with other theoretical predictions and examine the influences of these observables on the prediction of shell closures in each isotopic chain and the constraints they place on nuclear matter observables. In Fig. 2, we have plotted the total density distribution (sum of the proton ρ_p and the neutron ρ_n density) for ^{76}Fe and ^{86}Kr obtained from the NL3* and DD-ME1 interaction parameters as a representative case. One finds similar characteristics of the density for all nuclei considered in the present study. Further, a careful inspection shows a small enhancement in the surface region with an increase in proton number. In other words, the total density is extended towards the tail region in an isotonic chain and this ostensible distinction plays a significant role in the effective nuclear matter quantities.

The weight functions [in Eq. (17)] is interlinked with the nuclear matter observables, such as the symmetry energy, the neutron pressure and their related observables [63,64,67,70,71]. Following the CDFM approach, we briefly discuss the weight
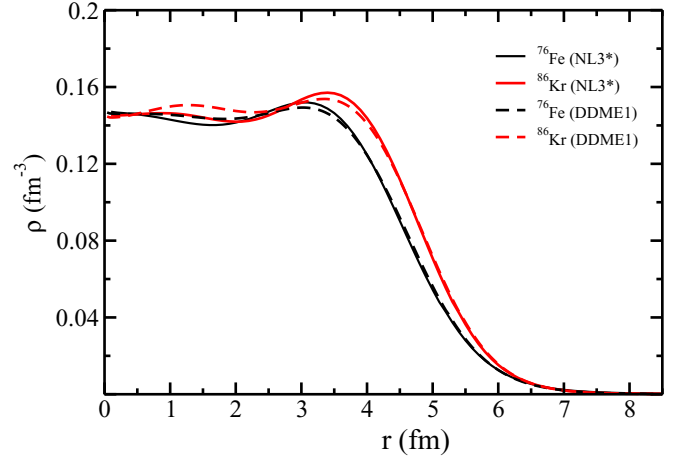

FIG. 2. The microscopic relativistic mean field with nonlinear NL3* and Dirac-Hartree-Bogoliubov with DD-ME1 total density distribution for ^{76}Fe and ^{86}Kr isotopes. See text for details.

function $|f(x)|^2$, i.e., in Eq. (17), which is directly associated with the density distribution of the finite nucleus. We have estimated the weight function of each nucleus using its total density $(\rho_p + \rho_n)$ distribution obtained from the relativistic mean field model. Here, we have given the $|f(x)|^2$ for ^{76}Fe and ^{86}Kr nuclei as representative cases, which are shown in Fig. 3. The weight function is the crucial quantity for describing the surface properties of the finite nucleus in terms of effective nuclear matter quantities. One can see from the figure, the weight function has a peak near the surface of the nuclear density density distribution. In other words, one finds a peak in the weight function ≈ 5 fm, which is due to contributions from the surface region of the nuclear density. For a better comprehension of this fact, one should compare the plots of the density distribution to those of the weight factor, i.e., see Figs. 2 and 3.
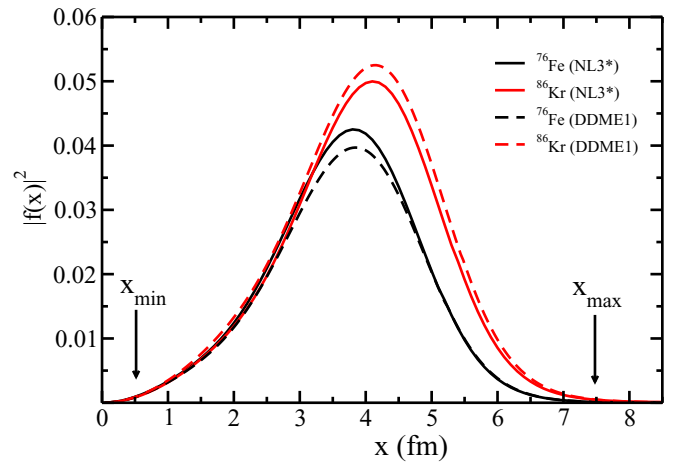

FIG. 3. The weight function $|f(x)|^2$ calculated for ^{76}Fe and ^{86}Kr isotopes by using the self-consistent NL3* and DD-ME1 total density distributions of these nuclei. The arrows stand for the minimum and maximum values of the integration limit taken in the subsequent calculations. See text for details.
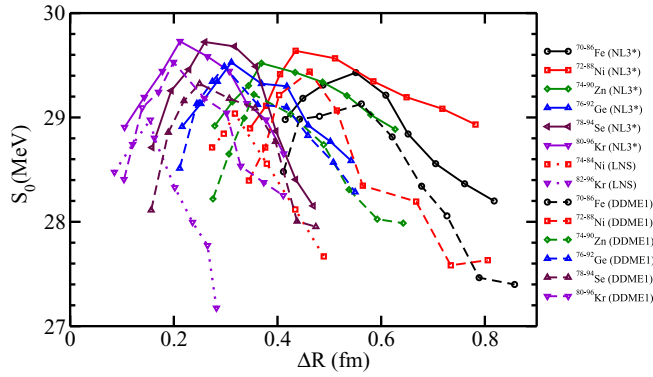
FIG. 4. The symmetry energy S_0 for $^{70-86}$Fe, $^{72-88}$Ni, $^{74-90}$Zn, $^{76-92}$Ge, $^{78-94}$Se, and $^{80-96}$Kr isotopes as a function of the neutron skin thickness ΔR as calculated using the RMF NL3* (solid line) and DD-ME1 (dashed line) interactions. The Skyrme-Hartree-Fock + BCS results for the LNS interaction [64,67] (dotted line) are given for comparison, where available. See the text for details.

FIG. 5. The symmetry energy S_0 and the quadrupole deformation β_2 for $^{70-86}$Fe, $^{72-88}$Ni, $^{74-90}$Zn, $^{76-92}$Ge, $^{78-94}$Se, and $^{80-96}$Kr isotopes as a function of neutron number N are given in the upper and lower panels, respectively. The calculated results from RMF NL3* (solid line) and DD-ME1 (dashed line) interactions are compared with the Skyrme-Hartree-Fock + BCS results for the LNS interaction [64,67] (dotted line) where available. See the text for details.

As we mentioned above, the objective of the present investigation is to study correlations between the neutron-skin thickness and effective nuclear matter properties such as the symmetry energy, neutron pressure (proportional to the slope of the bulk symmetry energy), and curvature in a given isotopic chain. Following Eq. (18), we first introduce the value of x_{min} at which the symmetry energy for nuclear matter $S^{NM}(x)$ changes sign from negative to positive at $x_{min} \geqslant x \leqslant x_{max}$ (see Fig. 3). In other words, the $S^{NM} < 0$ for the values of $x \leqslant x_{min}$ and $x \geqslant x_{max}$ in Eq. (18). Considering the basic principle of the CDFM, the domain of x should run from 0 to ∞, which incorporates the region of densities $\rho_0(x)$ from ∞ to 0, as well. At a point where the value of x is very small, in practice the estimate provides the values of density $\rho_0(x)$ that are much larger than the saturation density. To avoid such a nonphysical situation, i.e., a negative value of the symmetry energy, we include the value of $x \geqslant x_{min}$ for the lower limit and simultaneously exclude $x \geqslant x_{max}$ from the upper limit of the integration in Eq. (18). The estimated values of x_{min} and x_{max} of the integration are shown in Fig. 3.

C. The symmetry energy

The RMF calculations furnish principally nuclear structure properties, such as the quadrupole moment Q_{20}, nucleon density distribution $\rho(r_\perp, z) = \rho_p(r_\perp, z) + \rho_n(r_\perp, z)$, and the root-mean-square nuclear radii. We estimate the neutron skin thickness ΔR of nuclei in a given isotopic chain using the neutron and proton radii obtained from the relativistic mean field with the non-linear NL3* and density-dependent DD-ME1 interaction parameters. The symmetry energy S_0 for a given nucleus is calculated within the CDFM through the weight function $|f(x)|^2$ (obtained from the self-consistent density distribution) using Eq. (18). We show the symmetry energy S_0 as a function of neutron skin thickness in Fig. 4 for the $^{70-86}$Fe, $^{72-88}$Ni, $^{74-90}$Zn, $^{76-92}$Ge, $^{78-94}$Se, and $^{80-96}$Kr nuclei using the NL3* (solid line) and DD-ME1 (dashed line) interactions. The results obtained from a Skyrme-Hartree-Fock (SHF) + BCS with LNS interaction are also given for comparison, where
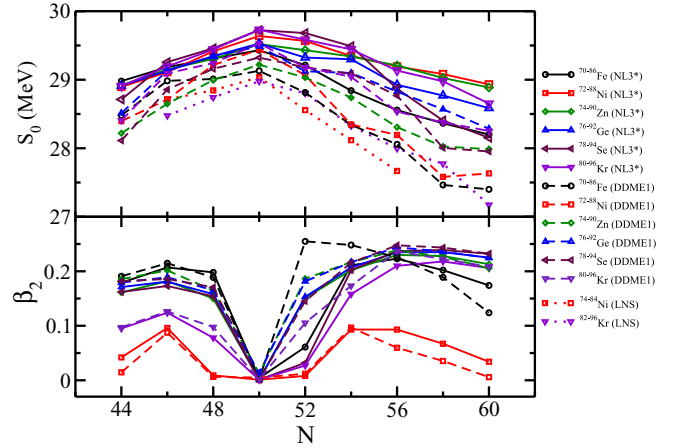
available. From the figure, we observe a smooth growth of S_0 up to the neutron number ($N = 50$) and then a linear decrease of S_0, where the neutron-skin thickness of the isotopes increases. The SHF displays a similar behavior of the symmetry energy with respect to the skin thickness. Careful inspection shows that the neutron skin thicknesses obtained from the RMF (NL3* and DD-ME1) are slightly larger when compared to those of the LNS interaction parameter. Further, the values of the S_0 for the relativistic interactions are slightly larger than the nonrelativistic LNS predictions, which can reflect on the nuclear matter characteristics [94,96].

The results exhibited in Fig. 4 are shown from an additional point of view in Fig. 5. In the upper and the lower panels of Fig. 5, we give the evolution of the symmetry energy and the quadrupole deformation β_0 as a function of the mass number, respectively. From the figure, we observe a similar peak of the symmetry energy at $N = 50$ for all the isotopic chains (see the upper panel of Fig. 5). One sees in Figs. 4 and 5 that S_0 varies by about 29.0 ± 1.0 MeV in the interval for the NL3* and DD-ME1 interaction parameters. The LNS interaction yields a values of S_0 smaller by ≈ 1 unit than the corresponding values of the relativistic interactions. The evolution of the symmetry energy is related to the development of the quadrupole moment as a function of the mass number, as displayed in the lower panel of Fig. 5. From the trajectory of the quadrupole deformation parameter β_2 as a function of mass number, one can see that the semi-magic isotopes corresponding to the neutron number $N = 50$ are spherical for both the NL3* and DD-ME1 interactions, while the open-shell isotopes within these isotopic chains have a prolate ground state configuration. Following Fig. 5, one can clearly see that the peak of the symmetry energy occurs for the closed shell nuclei that are spherical in shape. The open-shell nuclei display a slight decrease of the symmetry energy along the deformed shell. This represent a possible direction for further systematic
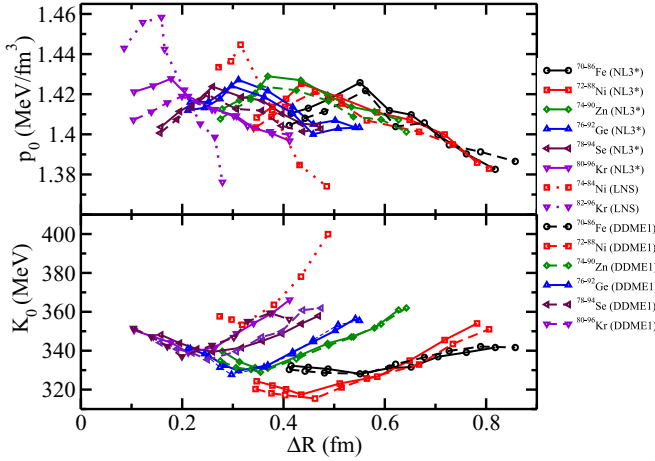
FIG. 6. The neutron pressure p_0 and the curvature K_0 for $^{70-86}$Fe, $^{72-88}$Ni, $^{74-90}$Zn, $^{76-92}$Ge, $^{78-94}$Se, and $^{80-96}$Kr isotopes as a function of neutron skin thickness ΔR using the nonlinear NL3* (solid line) and density-dependent DD-ME1 (dashed line) interactions are displayed in the upper and lower panels, respectively. The Skyrme-Hartree-Fock results for the LNS interaction [64,67] (dotted line) are given for comparison, where available. See text for details.

investigation of the isospin dependence of the nuclear equation of state.

D. Neutron pressure and curvature

Next, we illustrate a possible correlation of the neutron skin thickness ΔR with the neutron pressure p_0 and the curvature K_0, in Fig. 6. In Fig. 7, we plot the trajectory of p_0 and K_0 with neutron number for the Fe, Ni, Zn, Ge, Se, and Kr nuclei. The calculated results from the RMF NL3* (solid line) and
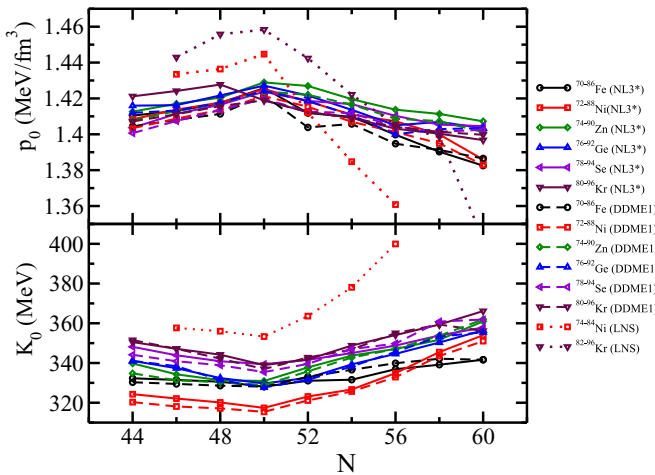

FIG. 7. The neutron pressure P_0 and the curvature K_0 for $^{70-86}$Fe, $^{72-88}$Ni, $^{74-90}$Zn, $^{76-92}$Ge, $^{78-94}$Se, and $^{80-96}$Kr isotopes as a function of mass number for the nonlinear NL3* and density-dependent DD-ME1 interactions are given in the upper and lower panels, respectively. The Skyrme-Hartree-Fock results for the LNS interaction [64,67] (dotted line) are also given for comparison, where available. See the text for details.

DD-ME1 (dashed line) interactions are given with the results of the nonrelativistic Skyrme-Hartree-Fock (LNS) interaction (dotted line) [64,67] for comparison, where available. From the figure it is clearly seen that the neutron skin thickness of the isotopes correlates almost linearly below and above the minimum with p_0 and K_0, as does S_0. Similar to the symmetry energy, here we also find a peak in the neutron pressure p_0 and a minimum in the curvature K_0 for semimagic nuclei at $N = 50$ for both interactions. Further, a slightly distorted transition is found in the linear correlation as compared to that of the symmetry energy curve. The small difference in the linear behavior indicates that the stability pattern is not as regular for the isotopic chain. As we have mentioned above, the peak follows a valley for a transition from a closed shell to an open shell nuclei. Here we have also found the same variation in the neutron pressure and curvature in the isotopic chains. It is worth mentioning that the decrease in S_0, p_0, and K_0 in the case of open-shell nuclei is due to the different occupancies of the single particle levels. Hence, we see that in general peaks are produced at shell closures. However, analysis of the precise dependence of the various peaks on the occupation number of specific shells will require further work. The results obtained from the nonlinear NL3* and density-dependent DD-ME1 interactions for p_0 and K_0 show a similar trend to that of the LNS force. More careful inspection shows that the results for p_0 and K_0 from our calculations are slightly smaller values than those of the LNS predictions. As we know, the magicity and/or shell closure (s) in an isotopic and/or isotonic chain are universal properties as far as the model used. Here, we get similar trends for nonlinear NL3* and density-dependent DD-ME1 interactions, which also qualitatively agree with the nonrelativistic NLS predictions. Hence, we can conclude, the results obtained in the present calculations are fairly model independent.

IV. SUMMARY AND CONCLUSIONS

In the present study, we have investigated possible relationships between the neutron skin thickness of neutron-rich nuclei and nuclear matter characteristics. A microscopic approach based on an axial deformed relativistic mean field with the nonlinear NL3* and density-dependent DD-ME1 interaction parameters has been used. Effective nuclear matter properties such as the symmetry energy S_0, the neutron pressure p_0, and the nuclear curvature parameter K_0 have been determined for finite nuclei. The coherent density functional method was used to provide a transparent and analytic manner of calculating the effective infinite nuclear matter quantities by means of a weight function. In the first step, we have obtained the ground state nuclear bulk properties such as the binding energies, quadrupole deformations, nuclear density distributions using the self-consistent microscopic RMF with the NL3* and DD-ME1 interactions. We have considered the even-even isotopic chains of Fe, Ni, Zn, Ge, Se, and Kr nuclei in the present analysis. The two neutron separation energies and the differential variation of the separation energies are also estimated from the microscopic binding energy for both the sets interaction parameters. From the separation energies, we found shell closures at $N = 50$ for all the isotopic chains

considered for both interactions. The neutron skin thickness and the weight function for each nucleus were estimated using the root-mean-square radius and the total density distribution, respectively.

In the second step, we have calculated effective infinite nuclear matter characteristics such as symmetry energy S_0, neutron pressure p_0 and curvature K_0 for the finite nuclei. For all of the isotopic chains, we found that there exists a strong correlation between the neutron skin thickness and the symmetry energy. We found a peak in S_0 in an isotopic chain, which corresponds to the semimagic isotopes at $N = 50$ and a spherical solution. An inflection-point transition appears for deformed nuclei at the spherical shell closures for the semimagic isotopes at $N = 50$ in the isotopic chain. In addition to these, a similar correlation between ΔR versus p_0 and ΔR versus K_0 has also been observed in the isotopic chains for both the NL3* and DD-ME1 sets of interaction parameters. The effect of the relative neutron-proton asymmetry on the evolution of the symmetry energy has been pointed out for these isotopes in the range $44 \leqslant N \leqslant 60$. We observe that the microscopic theoretical approach used is capable of predicting additional nuclear matter quantities in neutron-rich exotic nuclei and their connection to the surface properties of these nuclei. New exploratory results on giant resonances and the neutron skin in heavy nuclei and heavy-ion collisions could lead to new constraints on the nuclear symmetry energy, permitting an increased understanding of the physical quantities of nuclear systems.

[1] M. Leino, J. Äystö, T. Enqvist, P. Heikkinen, A. Jokinen, M. Nurmia, A. Ostrowski, W. H. Trzaska, J. Uusitalo, K. Eskola, P. Armbruster, and V. Ninov, Nucl. Instrum. Methods Phys. Res. B **99**, 653 (1995).

[2] C. J. Gross, T. N. Ginter, D. Shapira, W. T. Milner, J. W. McConnell, A. N. James, J. W. Johnson, J. Mas, P. F. Mantica, R. L. Auble, J. J. Das, J. L. Blankenship *et al.*, Nucl. Instrum. Methods Phys. Res. A **450**, 12 (2000).

[3] Z. Sun, W. L. Zhan, Z. Y. Guo, G. Xiao, and J. X. Li, Nucl. Instrum. Methods Phys. Res. A **503**, 496 (2003).

[4] M. Winkler, H. Geissel, H. Weick, B. Achenbach, K.-H. Behr, D. Boutin, A. Brü, M. Gleim, W. Hüller, C. Karagiannis, A. Kelic, B. Kindler *et al.*, Nucl. Instrum. Methods Phys. Res. B **266**, 4183 (2008).

[5] H. Sakurai, Nucl. Phys. A **805**, 526c (2008).

[6] A. C. Mueller and R. Anne, Nucl. Instrum. Methods Phys. Res. B **56**, 559 (1991).

[7] H. Geissel, P. Armbruster, K. H. Behr, A. Brünle, K. Burkard, M. Chen, H. Folger, B. Franczak, H. Keller, O. Klepper, B. Langenbeck, F. Nickel *et al.*, Nucl. Instrum. Methods Phys. Res. B **70**, 286 (1992).

[8] A. M. Rodin, S. V. Stepantsov, D. D. Bogdanov, M. S. Golovkov, A. S. Fomichev, S. I. Sidorchuk, R. S. Slepnev, R. Wolski, G. M. Ter-Akopian, Y. T. Oganessian, A. A. Yukhimchuk, V. V. Perevozchikov *et al.*, Nucl. Instrum. Methods Phys. Res. B **204**, 114 (2003).

[9] M. Thoennessen, Nucl. Phys. A **834**, 688c (2010).

[10] M. B. Tsang, J. R. Stone, F. Camera, P. Danielewicz, S. Gandolfi, K. Hebeler, C. J. Horowitz, J. Lee, W. G. Lynch, Z. Kohley, R. Lemmon, P. Möller, T. Murakami, S. Riordan, X. Roca-Maza, F. Sammarruca, A. W. Steiner, I. Vidaña, and S. J. Yennello, Phys. Rev. C **86**, 015803 (2012).

[11] P. Möller, W. D. Myers, H. Sagawa, and S. Yoshida, Phys. Rev. Lett. **108**, 052501 (2012).

[12] W. D. Myers, W. J. Swiatecki, and C. S. Wang, Nucl. Phys. A **436**, 185 (1985).

[13] K. Kolehmainen, M. Prakash, J. M. Lattimer, and J. Treiner, Nucl. Phys. A **439**, 535 (1985).

[14] M. Centelles, M. Del Estal, and X. Viñas, Nucl. Phys. A **635**, 193 (1998).

[15] J. M. Pearson, M. Farine, and J. Côté, Phys. Rev. C **26**, 267 (1982).

[16] F. Tondeur, M. Brack, M. Farine, and J. M. Pearson, Nucl. Phys. A **420**, 297 (1984).

[17] M. Warda, X. Viñas, X. Roca-Maza, and M. Centelles, Phys. Rev. C **80**, 024316 (2009).

[18] M. Warda, X. Viñas, X. Roca-Maza, and M. Centelles, Phys. Rev. C **81**, 054309 (2010).

[19] M. Warda, M. Centelles, X. Viñas, and X. Roca-Maza, Phys. Rev. C **89**, 064302 (2014).

[20] A. W. Steiner, M. Prakash, J. M. Lattimer, and P. J. Ellis, Phys. Rep. **411**, 325 (2005).

[21] A. E. L. Dieperink and P. Van Isacker, Eur. Phys. J. A **32**, 11 (2007).

[22] V. M. Kolomietz and A. I. Sanzhur, Eur. Phys. J. A **38**, 345 (2008).

[23] V. M. Kolomietz and A. I. Sanzhur, Phys. Rev. C **81**, 024324 (2010).

[24] N. Nikolov, N. Schunck, W. Nazarewicz, M. Bender, and J. Pei, Phys. Rev. C **83**, 034305 (2011).

[25] B. K. Agrawal, J. N. De, and S. K. Samaddar, Phys. Rev. Lett. **109**, 262501 (2012).

[26] S. J. Lee and A. Z. Mekjian, Phys. Rev. C **82**, 064319 (2010).

[27] B. K. Agrawal, D. Bandyopadhyay, J. N. De, and S. K. Samaddar, Phys. Rev. C **89**, 044320 (2014).

[28] L. Trippa, G. Colo, and E. Vigezzi, Phys. Rev. C **77**, 061304(R) (2008).

[29] D. T. Khoa and H. S. Than, Phys. Rev. C **71**, 044601 (2005).

[30] D. T. Khoa, H. S. Than, and D. C. Cuong, Phys. Rev. C **76**, 014603 (2007).

[31] D. V. Shetty and S. J. Yennello, Pramana **75**, 259 (2010).

[32] C. J. Horowitz, E. F. Brown, Y. Kim, W. G. Lynch, R. Michaels, A. Ono, J. Piekarewicz, M. B. Tsang, and H. H. Wolter, J. Phys. G: Nucl. Part. Phys. **41**, 093001 (2014).

[33] Z. H. Li, U. Lombardo, H.-J. Schulze, W. Zuo, L. W. Chen, and H. R. Ma, Phys. Rev. C **74**, 047304 (2006).

[34] J. Piekarewicz and M. Centelles, Phys. Rev. C **79**, 054311 (2009).

[35] I. Vidaña, C. Providência, A. Polls, and A. Rios, Phys. Rev. C **80**, 045806 (2009).

[36] F. Sammarruca and P. Liu, Phys. Rev. C **79**, 057301 (2009).

[37] S. K. Singh, M. Bhuyan, P. K. Panda, and S. K. Patra, J. Phys. G: Nucl. Part. Phys. **40**, 085104 (2013).

[38] S. K. Singh, S. K. Biswal, M. Bhuyan, and S. K. Patra, J. Phys. G: Nucl. Part. Phys. **41**, 055201 (2014).

[39] T. Nikšić, D. Vretenar, and P. Ring, Phys. Rev. C **78**, 034318 (2008).

[40] N. Van Giai, B. V. Carlson, Z. Ma, and H. Wolter, J. Phys. G **37**, 064043 (2010).

[41] E. N. E. van Dalen and H. Müther, Int. J. Mod. Phys. **19**, 2077 (2010).

[42] M. Bhuyan, Phys. Rev. C **92**, 034323 (2015).

[43] X. Roca-Maza, M. Centelles, X. Viñas, and M. Warda, Phys. Rev. Lett. **106**, 252501 (2011).

[44] S. Abrahamyan *et al.*, Phys. Rev. Lett. **108**, 112502 (2012).

[45] B.-A. Li, L.-W. Chen, and C. M. Ko, Phys. Rep. **464**, 113 (2008).

[46] L.-W. Chen, C. M. Ko, B.-A. Li, and G.-C. Yong, Int. J. Mod. Phys. E **17**, 1825 (2008).

[47] M. Colonna, J. Phys. Conf. Ser. **168**, 012006 (2009).

[48] V. Rodin, Prog. Part. Nucl. Phys. **59**, 268 (2007).

[49] S. K. Biswal, S. K. Singh, and S. K. Patra, Mod. Phys. Lett. A **30**, 1550097 (2015).

[50] P.-G. Reinhard and W. Nazarewicz, Phys. Rev. C **81**, 051303(R) (2010).

[51] V. V. Ivanovskaya, A. Zobelli, P. Wagner, M. I. Heggie, P. R. Briddon, M. J. Rayson, and C. P. Ewels, Phys. Rev. Lett. **107**, 065502 (2011).

[52] J. Piekarewicz *et al.*, Phys. Rev. C **85**, 041302(R) (2012).

[53] X. Roca-Maza *et al.*, Phys. Rev. C **88**, 024316 (2013).

[54] B. A. Brown, Phys. Rev. Lett. **119**, 122502 (2017).

[55] B.-J. Cai, B.-A. Li, and L.-W. Chen, Phys. Rev. C **94**, 061302(R) (2016).

[56] V. P. Psonis, Ch. C. Moustakidis, and S. E. Massen, Mod. Phys. Lett. A **22**, 1233 (2007).

[57] L. F. Roberts, G. Shen, V. Cirigliano, J. A. Pons, S. Reddy, and S. E. Woosley, Phys. Rev. Lett. **108**, 061103 (2012).

[58] H.-T. Janka, K. Langanke, A. Marek, G. Martínez-Pinedo, and B. Müller, Phys. Rep. **442**, 38 (2007).

[59] P. Danielewicz, R. Lacey, and W. G. Lynch, Science **298**, 1592 (2002).

[60] M. A. Famiano *et al.*, Phys. Rev. Lett. **97**, 052701 (2006).

[61] D. V. Shetty, S. J. Yennello, and G. A. Souliotis, Phys. Rev. C **76**, 024606 (2007).

[62] M. Centelles, X. Roca-Maza, X. Viñas, and M. Warda, Phys. Rev. Lett. **102**, 122502 (2009).

[63] P. Sarriguren, M. K. Gaidarov, E. M. de Guerra, and A. N. Antonov, Phys. Rev. C **76**, 044322 (2007).

[64] M. K. Gaidarov, A. N. Antonov, P. Sarriguren, and E. M. de Guerra, Phys. Rev. C **85**, 064319 (2012).

[65] B. A. Brown, Phys. Rev. Lett. **85**, 5296 (2000).

[66] S. Typel and B. A. Brown, Phys. Rev. C **64**, 027302 (2001).

[67] M. K. Gaidarov, A. N. Antonov, P. Sarriguren, and E. Moya de Guerra, Phys. Rev. C **84**, 034316 (2011).

[68] P. Van Isacker, M. A. Nagarajan, and D. D. Warner, Phys. Rev. C **45**, R13 (1992).

[69] S. Typel, Phys. Rev. C **89**, 064321 (2014).

[70] A. N. Antonov, V. A. Nikolaev, and I. Zh. Petkov, Bulg. J. Phys. **6**, 151 (1979).

[71] A. N. Antonov, V. A. Nikolaev, and I. Zh. Petkov, Z. Phys. A **304**, 239 (1982).

[72] A. N. Antonov, D. N. Kadrev, and P. E. Hodgson, Phys. Rev. C **50**, 164 (1994).

[73] K. A. Brueckner, J. R. Buchler, S. Jorna, and R. J. Lombard, Phys. Rev. **171**, 1188 (1968).

[74] K. A. Brueckner, J. R. Buchler, R. C. Clark, and R. J. Lombard, Phys. Rev. **181**, 1543 (1969).

[75] J. Boguta and A. R. Bodmer, Nucl. Phys. A **292**, 413 (1977).

[76] B. D. Serot and J. D. Walecka, in *Advances in Nuclear Physics*, edited by J. W. Negele and Erich Vogt (Plenum Press, New York, 1986), Vol 16, p. 1.

[77] W. Pannert, P. Ring, and J. Boguta, Phys. Rev. Lett. **59**, 2420 (1987).

[78] G. A. Lalazissis, S. Raman, and P. Ring, At. Data. Nucl. Data Tables **71**, 1 (1999).

[79] S. K. Patra, M. Bhuyan, M. S. Mehta, and Raj K. Gupta, Phys. Rev. C **80**, 034312 (2009).

[80] M. Bhuyan, S. K. Patra, and Raj K. Gupta, Phys. Rev. C **84**, 014317 (2011).

[81] P.-G. Reinhard, Rep. Prog. Phys. **52**, 439 (1989).

[82] P. Ring, Prog. Part. Nucl. Phys. **37**, 193 (1996).

[83] D. Vretenar, A. V. Afanasjev, G. A. Lalazissis, and P. Ring, Phys. Rep. **409**, 101 (2005).

[84] J. Meng, H. Toki, S. G. Zhou, S. Q. Zhang, W. H. Long, and L. S. Geng, Prog. Part. Nucl. Phys. **57**, 470 (2006).

[85] N. Paar, D. Vretenar, and G. Colo, Rep. Prog. Phys. **70**, 691 (2007).

[86] T. Nikšić, D. Vretenar, and P. Ring, Prog. Part. Nucl. Phys. **66**, 519 (2011).

[87] D. Logoteta, I. Vidaña, C. Providência, A. Polls, and I. Bombaci, J. Phys. Conf. Ser. **342**, 012006 (2012).

[88] X.-F. Zhao and H.-Y. Jia, Phys. Rev. C **85**, 065806 (2012).

[89] C. Fuchs, H. Lenske, and H. H. Wolter, Phys. Rev. C **52**, 3043 (1995).

[90] T. Niksic, D. Vretenar, P. Finelli, and P. Ring, Phys. Rev. C **66**, 024306 (2002).

[91] S. Typel and H. H. Wolter, Nucl. Phys. A **656**, 331 (1999).

[92] F. Hofmann, C. M. Keil, and H. Lenske, Phys. Rev. C **64**, 034314 (2001).

[93] B. V. Carlson and D. Hirata, Phys. Rev. C **62**, 054310 (2000).

[94] M. Dutra, O. Lourenço, S. S. Avancini, B. V. Carlson, A. Delfino, D. P. Menezes, C. Providência, S. Typel, and J. R. Stone, Phys. Rev. C **90**, 055203 (2014).

[95] B. M. Santos, M. Dutra, O. Lourenço, and A. Delfino, Phys. Rev. C **92**, 015210 (2015).

[96] M. Dutra, O. Lourenço, J. S. Sá Martins, A. Delfino, J. R. Stone, and P. D. Stevenson, Phys. Rev. C **85**, 035201 (2012).

[97] G. A. Lalazissis, S. Karatzikos, R. Fossion, D. Pena Arteaga, A. V. Afanasjev, and P. Ring, Phys. Lett. B **671**, 36 (2009).

[98] B. D. Serot and J. D. Walecka, Int. J. Mod. Phys. E **06**, 515 (1997).

[99] Y. K. Gambhir, P. Ring, and A. Thimet, Ann. Phys. (NY) **198**, 132 (1990).

[100] R. J. Furnstahl, J. J. Rusnak, and B. D. Serot, Nucl. Phys. A **632**, 607 (1998).

[101] M. Jaminon and C. Mahaux, Phys. Rev. C **40**, 354 (1989).

[102] M. Bender, P.-H. Heenen, and P.-G. Reinhard, Rev. Mod. Phys. **75**, 121 (2003).

[103] B. A. Nikolaus, T. Hoch, and D. G. Madland, Phys. Rev. C **46**, 1757 (1992).

[104] T. Burvenich, D. G. Madland, J. A. Maruhn, and P.-G. Reinhard, Phys. Rev. C **65**, 044308 (2002).

[105] R. Brockmann and H. Toki, Phys. Rev. Lett. **68**, 3408 (1992).

[106] G. A. Lalazissis, J. König, and P. Ring, Phys. Rev. C **55**, 540 (1997).

[107] S. Karatzikos, A. V. Afanasjev, G. A. Lalazissis, and P. Ring, Phys. Lett. B **689**, 72 (2010).

[108] J. Y. Zeng and T. S. Cheng, Nucl. Phys. A **405**, 1 (1983).

[109] H. Molique and J. Dudek, Phys. Rev. C **56**, 1795 (1997).

[110] Z.-H. Zhang, J.-Y. Zeng, E.-G. Zhao, and S.-G. Zhou, Phys. Rev. C **83**, 011304(R) (2011).

[111] T. V. Nhan Hao, P. Quentin, and L. Bonneau, Phys. Rev. C **86**, 064307 (2012).

[112] G. A. Lalazissis, D. Vretenar, P. Ring, M. Stoitsov, and L. M. Robledo, Phys. Rev. C **60**, 014310 (1999).

[113] G. A. Lalazissis, D. Vretenar, and P. Ring, Nucl. Phys. A **650**, 133 (1999).

[114] J. Dobaczewski, H. Flocard, and J. Treiner, Nucl. Phys. A **422**, 103 (1984).

[115] D. G. Madland and J. R. Nix, Nucl. Phys. A **476**, 1 (1988).

[116] P. Möller and J. R. Nix, At. Data Nucl. Data Tables **39**, 213 (1988).

[117] M. Wang, G. Audi, A. H. Wapstra, F. G. Kondev, M. Mac-Cormick, X. Xu, and B. Pfeiffer, Chen. Phys. C **36**, 1603 (2012).

[118] I. Angeli and K. P. Marinova, At. Data Nucl. Data Tables **99**, 69 (2013).

[119] B. Pritychenko, J. Choquette, M. Horoi, B. Karamy, and B. Singh, At. Data Nucl. Data Tables **98**, 798 (2012).